ChemComm

COMMUNICATION

View Article Online
View Journal

Cite this: DOI: 10.1039/d6cc00397d

Received 21st January 2026,
Accepted 19th February 2026

DOI: 10.1039/d6cc00397d

rsc.li/chemcomm

Nickel(II) driven activity enhancement of a donor–acceptor porous organic polymer for selective photoreduction of carbon dioxide

A John David,[a] Nandini M Gotgi,[b] Gopika Udayakumar,[a] A Hameed Ibrahim,[a] Abhilash Pullanchiyodan,*[a] Debashis Ghosh*[c] and Anjan Das*[a]

We report the design and synthesis of porous organic polymers (Py-DPEN) as a photocatalyst for the photoreduction of CO_2 to carbon monoxide (CO). Incorporation of Ni(II) drastically enhanced the photocatalytic activity under visible light irradiation (70 W m^{-2}, 470 nm), resulting in a significantly higher CO yield (38 μmol) with excellent selectivity. This pronounced improvement demonstrates the crucial role of Ni(II) in driving CO_2 conversion using TEOA as a sacrificial electron donor in an acetonitrile–water medium. Comprehensive characterization, photocatalytic performance evaluation, and product selectivity studies confirm the outstanding efficiency of the system and provide valuable insights for the rational design of sustainable energy conversion catalysts.

The increasing levels of atmospheric carbon dioxide (CO_2) due to anthropogenic activities have led to severe environmental challenges, including global warming and climate change.[1] To address this issue, the development of innovative and sustainable technologies for CO_2 capture, utilization, and conversion is required. Among various strategies, photocatalytic reduction of CO_2 into value-added chemicals using solar energy has garnered significant interest as a promising approach to mitigate CO_2 emissions and produce useful carbon-based fuels.[2]

Photocatalytic CO_2 reduction mimics natural photosynthesis by harnessing solar energy to convert CO_2 into valuable chemical feedstocks. However, the high bond dissociation energy of the C=O bond in CO_2 makes this process energy-intensive, especially when aiming to produce energy-rich products such as CO, HCOOH, HCHO, CH_3OH, and CH_4.[3] Moreover, CO_2 reduction involves multiple proton-coupled electron transfer steps, which complicates the development of efficient photocatalysts.[4] Among the various reduction pathways, the selective conversion of CO_2 to CO is particularly appealing due to its relevance in syngas production – a two-electron reduction process. Additionally, CO serves as an essential intermediate for synthesizing higher-order products such as CH_3OH, C_2H_5OH, and other valuable hydrocarbons using the well-established Fischer–Tropsch process.[5]

Among the various heterogeneous photocatalytic materials,[6] porous organic polymers (POPs)[7] have emerged as a promising class of porous materials with tuneable structures, high surface areas, and excellent chemical stability. In the context of photocatalysis, POPs offer several advantages, such as robust chemical frameworks, extended π-conjugated networks, and permanent porosity, which are important for efficient heterogeneous photocatalytic CO_2 reduction.[8] The incorporation of transition metal atoms, such as Nickel, within the POP backbone can significantly enhance the catalytic activity by acting as a redox-active centre as well as CO_2 binding sites, promoting selective CO_2 reduction pathways.[9]

In this study, we report the synthesis and characterization of a pyrene-based π-conjugated POP (Py-DPEN) and investigated how the incorporation of Ni(II) in the organic framework enhances the photocatalytic activity for selective photoreduction of carbon dioxide (Fig. 1). We presumed that the synergistic

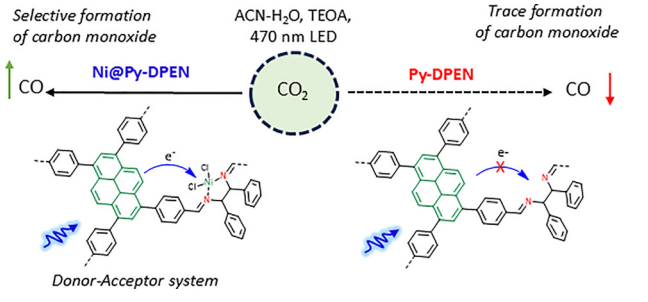

Fig. 1 Selective photoreduction of carbon dioxide.

[a] Department of Chemistry, SRM Institute of Science and Technology, Kattankulathur, Chennai, Tamil Nadu, India 603203. E-mail: anjand@srmist.edu.in
[b] Department of Chemistry, St. Joseph's University, 36 Lalbagh Road, Bengaluru-560027, Karnataka, India
[c] Department of Chemistry, R.D. & D.J. College, Munger 811201, Bihar, India

electron transfer between the light-harvesting pyrene-based organic framework (donor) and the redox-active Ni centres (acceptor) effectively couples the catalytic cycles.[10]

The structural characteristics of Py-DPEN and Ni@Py-DPEN are explored using a combination of spectroscopic and microscopic techniques, while photocatalytic performance is assessed through controlled CO_2 reduction experiments. ^{13}C CP-MAS NMR spectra confirmed the formation of the imine bonds in the materials. The signal corresponding to the (C═N) is at 160.9 ppm (Fig. S2). The crystalline structure and ordered nature of Py-DPEN and Ni@Py-DPEN were confirmed by powder X-ray diffraction (PXRD) analysis (Fig. S3). The incorporation of Ni(II) centres into Py-DPEN was confirmed by comparing the IR spectra of Py-DPEN and Ni@Py-DPEN. A significant red shift in the C═N stretching frequency was observed in the IR spectrum of Ni@Py-DPEN, appearing at 1574 cm^{-1}, compared to 1614 cm^{-1} for Py-DPEN (Fig. 2a). Apart from this shift, the IR spectrum of Ni@Py-DPEN showed no major changes relative to Py-DPEN, indicating that the backbone structure was retained during the post-metalation process. The Brunauer–Emmett–Teller (BET) surface area calculated for the Py-DPEN is 328 $m^2\ g^{-1}$ and that for Ni@Py-DPEN is 164 $m^2\ g^{-1}$ (Fig. S5). Transmission electron microscopy (TEM) and scanning electron microscopy (SEM) images confirmed the presence of microrod and clustered structures in the Ni@Py-DPEN (Fig. 2c and d). Moreover, these images indicated that no metal oxides

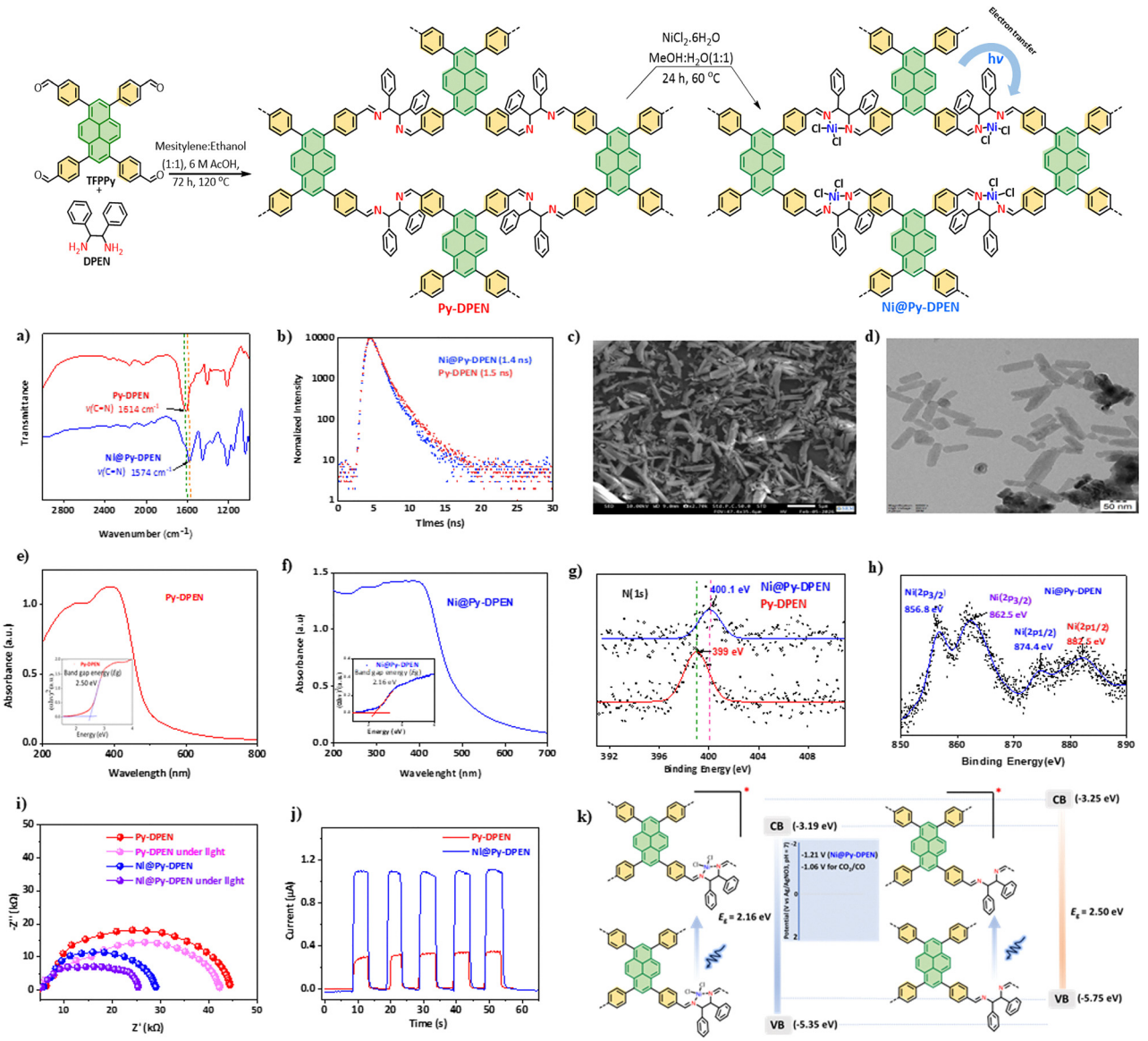

Fig. 2 (a) IR spectra of Py-DPEN and Ni@Py-DPEN; (b) lifetime of Py-DPEN and Ni@Py-DPEN; (c) SEM image of Ni@Py-DPEN; (d) TEM image of Ni@Py-DPEN; (e) UV-Vis (Tauc plot) of Py-DPEN; (f) UV-Vis (Tauc plot) of Ni@Py-DPEN; (g) comparative N(1s) XPS analysis of Py-DPEN and Ni@Py-DPEN (390 eV to 414 eV region); (h) Ni(2p) XPS analysis of Ni@Py-DPEN (850 eV to 890 eV region); (i) EIS Nyquist plot of Py-DPEN and Ni@Py-DPEN in the presence and absence of light; (j) transient photocurrent responses of Py-DPEN and Ni@Py-DPEN; (k) the light absorbing ability of Py-DPEN and Ni@Py-DPEN and arrangements of the valence band (VB) and conduction band (CB); standard reduction potentials of Ni@Py-DPEN and CO_2/CO vs $Ag/AgNO_3$.[2b]

Table 1 Electrochemical data[a]

Catalyst	Reduction potential (E_{red})	Conduction band energy [$E_{CB} = -e(E_{red} + 4.40)$] (eV)	Band gap energy (E_g) (eV)	Valence band energy [$E_{VB} = E_{CB} - E_g$] (eV)
Ni@Py-DPEN	−1.21, −1.81	−3.19	2.16	−5.35
Py-DPEN	−1.15, −1.95	−3.25	2.50	−5.75

[a] *E vs.* $Ag/AgNO_3$ (10 mM) measured in CH_3CN containing 0.1 M $TBAPF_6$.

or nanoparticles formed during the incorporation of $NiCl_2$ into the POP framework. Energy-dispersive X-ray (EDX) mapping, based on both TEM and SEM, further demonstrated a uniform distribution of Ni throughout the Ni@Py-DPEN POP matrix (Fig. S9 and 10). There is a large decrease in charge-transfer resistance (R_{ct}) in Ni@Py-DPEN (28 kohm) compared to Py-DPEN (45 kohm), confirming efficient electron transfer in Ni@Py-DPEN, and upon light excitation the R_{ct} decreases further due to facile electron transfer in the excited state (Fig. 2i). Additionally, we observed very high transient photocurrent for Ni@Py-DPEN (1.1 μA) compared to Py-DPEN (0.3 μA) (Fig. 2j).

X-ray photoelectron spectroscopy (XPS) analysis confirmed the successful incorporation of Ni(II) into the Py-DPEN framework. Ni@Py-DPEN exhibited characteristic Ni $2p_3/_2$ and Ni $2p_1/_2$ peaks at 856.8 and 874.4 eV, along with satellite peaks at 862.5 and 880.9 eV, consistent with the Ni(II) oxidation state and with no evidence of Ni(0) or NiO impurities (Fig. 2h). Comparison of the high-resolution N1s spectra showed a positive shift from 399.1 to 400.1 eV upon metalation (Fig. 2g), indicating coordination of Ni(II) *via* imine nitrogen atoms, while spectral deconvolution supported the expected nitrogen environments (Fig. S8).[11] These results confirm selective Ni(II) coordination without structural alteration or extraneous metal species. Inductively coupled plasma-optical emission spectrometry (ICP-OES) analysis indicated that 2.64 wt% of Ni content was present in the Ni@Py-DPEN POP and only 0.08% leached after the photocatalytic run. TGA further demonstrated excellent thermal stability of both Py-DPEN and Ni@Py-DPEN up to ~300 °C after $NiCl_2$ incorporation (Fig. S4).

The UV-Vis spectrum of Ni@Py-DPEN POP showed a broad absorption from 370–500 nm, indicating strong visible-light harvesting (Fig. 2f). The red shift relative to the solid-state UV-vis spectra of TFPPy (donor) and Ni@DPEN (acceptor) (Fig. S7) confirms the formation of a donor–acceptor complex. The Tauc plot (Fig. 2f inset) revealed a reduced band gap of 2.16 eV for Ni@Py-DPEN compared to 2.50 eV for Py-DPEN (Fig. 2e), demonstrating that incorporating the Ni(II) centre enhances electron delocalization and lowers the band gap, improving photocatalytic efficiency. The photoluminescence spectrum reveals that, upon excitation at 390 nm, Ni@Py-DPEN POP exhibits an emission peak at 440 nm (Fig. S6). Time-resolved emission measurements indicate an average excited-state lifetime of 1.4 ns for Ni@Py-DPEN POP, compared to 1.5 ns for Py-DPEN POP (Fig. 2b). This slight reduction in lifetime from Py-DPEN POP to Ni@Py-DPEN POP provides clear evidence of efficient energy or electron transfer from the POP backbone to the Ni centre.

The electrochemical behaviour of Ni@Py-DPEN was examined by cyclic voltammetry (CV) in CH_3CN using a glassy carbon working electrode, a platinum counter, and an $Ag/AgNO_3$ reference electrode (Table 1). Two irreversible redox waves appeared at −1.21 V and −1.81 V vs $Ag/AgNO_3$ under Ar (Fig. 3a). In comparison, the Py-DPEN-modified electrode showed similar irreversible waves at −1.15 V and −1.95 V, indicating that the cathodic redox processes originate from the ligand sites. In CH_3CN/H_2O (90/10, v/v), both electrodes exhibited broad irreversible waves near −1.05 V under Ar (Fig. S11). Upon CO_2 saturation (20 min sparging), Ni@Py-DPEN displayed a strong catalytic current starting at −1.25 V (Fig. 3b), whereas Py-DPEN POP showed no catalytic response up to −2.0 V (Fig. S12). These results indicate that the Ni(II) centres in Ni@Py-DPEN POP are responsible for CO_2 reduction.

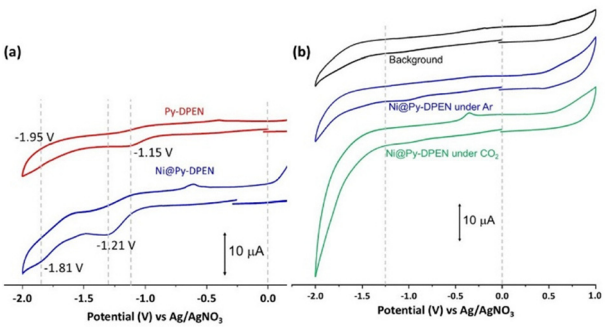

Fig. 3 (a) Cyclic voltammogram of Ni@Py-DPEN POP (blue) and Py-DPEN (red) (drop-casted on glassy carbon electrode) in CH_3CN under Ar, for all measurements, 0.1 M $TBAPF_6$ was used as a supporting electrolyte, and $Ag/AgNO_3$ (10 mM, in CH_3CN) was taken as a reference electrode; scan rate: 100 mV s^{-1}; (b) cyclic voltammogram of Ni@Py-DPEN POP (drop-casted on glassy carbon electrode) in $CH_3CN–H_2O$ (9 : 1 v/v) under Ar (blue) and CO_2 (green) atmospheres, and background (black). For all measurements, 0.1 M $TBAPF_6$ was used as a supporting electrolyte, and $Ag/AgNO_3$ (10 mM, in CH_3CN) was taken as a reference electrode; scan rate: 100 mV s^{-1}.

Table 2 Photocatalytic reaction results[a]

Entry	Product	Ni@Py-DPEN (μmol)	Py-DPEN (μmol)	Ni@Py-DPEN[b] (μmol)
1	CO	38.0	8.90	8.19
2	CH_4	4.5	1.66	1.17
3[c]	CO	0	—	—

[a] Irradiated with a blue LED at λ_{ex} = 470 nm (light power = 70 W m^{-2}). Formation of CO and CH_4, during the photoirradiation of a CO_2-saturated solution containing 3 mg of POP in $CH_3CN–H_2O–TEOA$ (9 : 1 : 2 v/v, 4.0 mL). [b] Ni@Py-DPEN (3 mg) in $CH_3CN–TEOA$ (4 : 1 v/v, 4.0 mL) at 298 K. HCOOH and H_2 were not detected for all reactions. [c] In an inert atmosphere (under N_2).

As a typical run, a CH_3CN–H_2O–TEOA (9 : 1 : 2 v/v) solution containing Ni@Py-DPEN (or Py-DPEN) (3 mg) was irradiated at λ_{ex} = 470 nm (light power = 70 W m^{-2}) under a CO_2 atmosphere (Table 2). The main product was CO with CH_4 formation to a lesser degree in either solution (the selectivity of CO was found to be 89.4% and 84.2%, respectively), and HCOOH and H_2 were not detected (Table S1). The photochemical results clearly indicate the importance of the Ni centre in the POP material for CO_2 reduction. Additionally, we have tested photochemical CO_2 reduction using the Ni@Py-DPEN catalyst (3 mg), in CH_3CN–TEOA (4 : 1 v/v) solution under similar conditions with CO (8.19 μmol) and CH_4 (1.17 μmol) (Table 2; as well as Table S1). Interestingly, the yields of CO and CH_4 were much less in CH_3CN–TEOA (4 : 1 v/v) than that of CH_3CN–H_2O–TEOA (9 : 1 : 2 v/v). The availability of the proton source in CH_3CN–H_2O–TEOA solution might be the main reason for the high product formation.[9] The apparent quantum yield of CO was found to be Φ_{CO} = 1.98% and 0.426% with Ni@Py-DPEN POP in CH_3CN–TEOA–H_2O and CH_3CN–TEOA, respectively (see the SI for details).

Based on the above experimental evidence, a possible reaction mechanism has been proposed (Fig. S16). The reductive quenching of the excited state of the pyrene part of Ni@Py-DPEN POP by TEOA should ($E_{TEOA/TEOA^{+\bullet}}$ = +0.34 V)[12] allow smooth transfer of an electron from $Pyrene^{-\bullet}$ to the Ni(II) catalyst site, converting Ni(II) into Ni(I). The Ni(I) might bind with CO_2 and further one electron addition followed by one proton addition should induce CO_2 reduction *via* the proton coupled electron transfer pathway (PCET).[13] After CO_2 reduction occurs, the Ni(II) catalyst site returns to its Ni(II) state, completing the cycle. The binding and activation of CO_2 by Ni has been well studied by DFT calculation.[14]

We report a donor–acceptor imine-based metallo-porous organic polymer (POP) for visible-light-driven CO_2 reduction with good selectivity. The conjugated framework minimizes the band gap upon Ni(II) incorporation, enhancing charge separation and enabling efficient charge-transfer-driven catalysis. In this architecture, the pyrene derivative acts as the light-harvesting material, while Ni@DPEN functions as the redox-active acceptor; their spatial integration within the POP pores promotes rapid excited-state electron transfer to the Ni sites in the presence of triethanolamine as a sacrificial electron donor. This synergistic design drives multielectron CO_2 to CO conversion with 89.4% selectivity, delivering 38 μmol of CO in 6 h using triethanolamine in an acetonitrile–water mixture as the electron donor. Electrochemical studies confirm the redox behaviour of Ni@Py-DPEN POP, as well as its effectiveness towards CO_2 photoreduction.

AD and DG designed the project. AJD and NMG performed experiments. AD, AP, and DG wrote the manuscript. AD acquired the funding and directed the research.

Conflicts of interest

There are no conflicts to declare.

Data availability

The supplementary information (SI) includes all experimental details, including the synthesis and characterization of the materials reported in this study. See DOI: https://doi.org/10.1039/d6cc00397d.

Acknowledgements

A. J. D. and H. I. acknowledge the Department of Chemistry, SRM institute of Science and Technology, Kattankulathur, Tamil Nadu, India, for financial support through an Institute Doctoral Fellowship. A. D. sincerely acknowledges SRMIST for the seed grant (No. SRMIST/R/AR(A/SERI2024/174/14–342), the Anusandhan National Research Foundation (ANRF-ECRG, Grant No. ANRF/ECRG/2024/003299/CS), and the RSC-Newton International Alumni Fellowship (AL\24100051) for the financial support. D. G. sincerely thanks the ANRF (Grant No. SUR/2022/000359) for financial support. We also thank the SRM Central Instrumentation Facility (SRM-SCIF) and the Nano Research Centre (SRM-NRC) for providing access to instrumentation facilities.

References

1 (*a*) K. S. Song, P. W. Fritz and A. Coskun, *Chem. Soc. Rev.*, 2022, **51**, 9831–9852; (*b*) J. Low, B. Cheng and J. Yu, *Appl. Surf. Sci.*, 2017, **392**, 658–686; (*c*) H. A. Patel and C. T. Yavuz, *Faraday Discuss.*, 2015, **183**, 401–412; (*d*) M. Zhou, Z. Wang, A. Mei, Z. Yang, W. Chen, S. Ou, S. Wang, K. Chen, P. Reiss, K. Qi, J. Ma and Y. Liu, *Nat. Commun.*, 2023, **14**, 2473; (*e*) S. Zhu, X. Li, X. Jiao, W. Shao, L. Li, X. Zu, J. Hu, J. Zhu, W. Yan, C. Wang, Y. Sun and Y. Xie, *Nano Lett.*, 2021, **21**, 2324–2331; (*f*) K. Sun, Y. Qian and H.-L. Jiang, *Angew. Chem., Int. Ed.*, 2023, **62**, e202217565; (*g*) P. Verma, F. A. Rahimi, D. Samanta, A. Kundu, J. Dasgupta and T. K. Maji, *Angew. Chem., Int. Ed.*, 2022, **61**, e202116094; (*h*) K. Khaletskaya, A. Pougin, R. Medishetty, C. Rösler, C. Wiktor, J. Strunk and R. A. Fischer, *Chem. Mater.*, 2015, **27**, 7248–7257; (*i*) S. Karmakar, S. Barman, F. A. Rahimi, D. Rambabu, S. Nath and T. K. Maji, *Nat. Commun.*, 2023, **14**, 4508.

2 (*a*) X. Yu, Z. Yang, B. Qiu, S. Guo, P. Yang, B. Yu, H. Zhang, Y. Zhao, X. Yang, B. Han and Z. Liu, *Angew. Chem., Int. Ed.*, 2019, **58**, 632–636; (*b*) A. Singh, P. Verma, D. Samanta, A. Dey, J. Dey and T. K. Maji, *J. Mater. Chem. A*, 2021, **9**, 5780–5786.

3 (*a*) X. Yao, K. Chen, L.-Q. Qiu, Z.-W. Yang and L.-N. He, *Chem. Mater.*, 2021, **33**, 8863–8872; (*b*) P. Verma, A. Singh, F. A. Rahimi, P. Sarkar, S. Nath, S. K. Pati and T. K. Maji, *Nat. Commun.*, 2021, **12**, 7313; (*c*) K.-G. Liu, F. Bigdeli, A. Panjehpour, A. Larimi, A. Morsali, A. Dhakshinamoorthy and H. Garcia, *Coord. Chem. Rev.*, 2023, **493**, 215257.

4 Z. Chen, Y. Hu, J. Wang, Q. Shen, Y. Zhang, C. Ding, Y. Bai, G. Jiang, Z. Li and N. Gaponik, *Chem. Mater.*, 2020, **32**, 1517–1525.

5 (*a*) D. K. Chauhan, N. Sharma and K. Kailasam, *Mater. Adv.*, 2022, **3**, 5274–5298; (*b*) S. Wang, B. Y. Guan and X. W. D. Lou, *J. Am. Chem. Soc.*, 2018, **140**, 5037–5040.

6 (*a*) S. Sun, M. Watanabe, J. Wu, Q. An and T. Ishihara, *J. Am. Chem. Soc.*, 2018, **140**, 6474–6482; (*b*) S. Neaţu, J. A. Macia-Agullo, P. Concepcion and H. Garcia, *J. Am. Chem. Soc.*, 2014, **136**, 15969–15976; (*c*) A. Bathla, J. Lee, S. A. Younis and K.-H. Kim, *Mater. Today Chem.*, 2022, **24**, 100870.

7 (*a*) R. Das, R. Paul, A. Parui, A. Shrotri, C. Atzori, K. A. Lomachenko, A. K. Singh, J. Mondal and S. C. Peter, *J. Am. Chem. Soc.*, 2023, **145**, 422–435; (*b*) T. Kajiwara, M. Fujii, M. Tsujimoto, K. Kobayashi, M. Higuchi, K. Tanaka and S. Kitagawa, *Angew. Chem., Int. Ed.*, 2016, **55**, 2697–2700; (*c*) Z. Zhong, X. Wang and B. Tan, *Chem. – Eur. J.*, 2025, **31**, e202404089; (*d*) W.-J. Wang and K. Chen, *Chin. Chem. Lett.*, 2025, **36**, 109998; (*e*) H. Ali, Y. Orooji, A. Y. A. Alzahrani, M. H. A. Mughram, A. M. Abu-Dief, I. Omar, A. Hayat, D. Yue and Y. Xu, *Coord. Chem. Rev.*, 2025, **543**, 216884.

8 (*a*) G. M. Eder, D. A. Pyles, E. R. Wolfson and P. L. McGrier, *Chem. Commun.*, 2019, **55**, 7195–7198; (*b*) C. Sarkar, R. Paul, D. Q. Dao, S. Xu, R. Chatterjee, S. C. Shit, A. Bhaumik and J. Mondal, *ACS Appl. Mater. Interfaces*, 2022, **14**, 37620–37636; (*c*) G. Mukherjee, J. Thote, H. B. Aiyappa, S. Kandambeth, S. Banerjee, K. Vanka and R. Banerjee, *Chem. Commun.*, 2017, **53**, 4461–4464; (*d*) Y. Ma, X. Yi, S. Wang, T. Li, B. Tan, C. Chen, T. Majima, E. R. Waclawik, H. Zhu and J. Wang, *Nat. Commun.*, 2022, **13**, 1400.

9 (*a*) K. Niu, Y. Xu, H. Wang, R. Ye, H. L. Xin, F. Lin, C. Tian, Y. Lum, K. C. Bustillo, M. M. Doeff, M. T. M. Koper, J. Ager, R. Xu and H. Zheng, *Sci. Adv.*, 2017, **3**, e1700921; (*b*) N. Zahir, V. Rajangam, S. S. Kalanur, S. I. Nikitenko and B. G. Pollet, *Energy Environ. Mater.*, 2025, **8**, e70014.

10 N. Xu, Y. Diao, X. Qin, Z. Xu, H. Ke and X. Zhu, *Dalton Trans.*, 2020, **49**, 15587.

11 A. Jati, S. Dam, S. Kumar, K. Kumar and B. Maji, *Chem. Sci.*, 2023, **14**, 8624–8634.

12 B. Kurpil, Y. Markushyna and A. Savateev, *ACS Catal.*, 2019, **9**, 1531–1538.

13 D. Ghosh, H. Takeda, D. C. Fabry, Y. Tamaki and O. Ishitani, *ACS Sustainable Chem. Eng.*, 2019, **7**, 2648–2657.

14 (*a*) S. Liang, X. Zhong, Z. Zhong, H. Deng and W.-Y. Wong, *Appl. Catal., B*, 2023, **337**, 122958; (*b*) J. Song, E. L. Klein, F. Neese and S. Ye, *Inorg. Chem.*, 2014, **53**, 7500–7507; (*c*) P. Yadav, S. Kumar, N. Velankanni, T. D. Kühne, S. Gosavi, R. K. M. Raghupathy, R. Bhosale, G. Held, M. Shelke and S. Ogale, *J. Phys. Energy*, 2024, **6**, 025019.